EUROPEAN ORGANIZATION FOR NUCLEAR RESEARCH

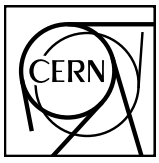

ALICE-INT-2012-xxx
July 20, 2012

Two-proton correlations in Pb–Pb collisions at $\sqrt{s_{NN}} = 2.76$ TeV from the ALICE experiment at the LHC

Maciej Szymański[1]
Adam Kisiel[1]

1. Warsaw University of Technology

Email: Maciej.Szymanski@cern.ch
Adam.Kisiel@cern.ch

Abstract

Correlations of all combinations of pairs of protons and antiprotons are measured in Pb–Pb collisions at $\sqrt{s_{NN}} = 2.76$ TeV in the ALICE experiment. One-dimensional pp, $\bar{\mathrm{p}}\bar{\mathrm{p}}$ and $\mathrm{p}\bar{\mathrm{p}}$ correlation functions are formed in three centrality and two pair transverse momentum ranges. The femtoscopic parameters for the radius of the proton source are extracted. The fit includes final-state interactions (strong and Coulomb) and quantum statistics, in case of identical pairs of (anti)protons. Also, the fit takes into account residual correlations coming from pΛ system. Two-proton correlations show an increase of the radius with increasing multiplicity and slight decrease of the radius with increasing pair transverse momentum.

1 Introduction

In the analysis, we present the measurements of two-proton correlations in Pb–Pb collisions at $\sqrt{s_{NN}} =$ 2.76 TeV registered by the ALICE experiment. The method of two-particle correlations (commonly referred to as *femtoscopy*) allows for extracting the space-time characteristics of the emitting source created in heavy-ion collision. Correlations of identical bosons have been usually used to perform this study. In particular, the ALICE Collaboration has recently carried out the analysis of two-pion correlations in central Pb–Pb collisions [1]. Proton-proton correlations have also been measured for the broad range of the energies of heavy-ion collisions, especially in Au+Au collisions at $\sqrt{s_{NN}} = 200$ GeV by the STAR experiment at RHIC [2].

The main motivation to carry out two-proton femtoscopic study is to complement information about the source size deduced from the correlations of pions and kaons. The analysis provides a test of the hydrodynamic prediction of the transverse mass scaling and gives a possibility for checking if the collectivity also includes baryons. Due to the fact that feed-down from weak decays cannot be neglected in high-energy heavy-ion collisions, the effects of residual correlations related with the pΛ system should be taken into account in the study of proton femtoscopy. Because of the low decay momentum of Λ decay into p and π^- with respect to the mass of proton, femtoscopic correlations between a Λ and a primary proton might still be detected for a pair consisting of a primary proton and the proton from Λ. Furthermore, proton-antiproton correlations should be investigated as a proof that the influence of final-state interaction (the annihilation) may contribute to lowering multiplicities of protons observed at LHC energies, with respect to predictions from chemical models.

2 Data analysis

2.1 Data sample

2.1.1 Real data

The data used in this note come from Pb–Pb collisions recorded by the ALICE experiment during the 2011 run at the LHC (production LHC11h, pass 2). Analysis Object Data (AOD095) files have been used in studies. About 35 milion events have been analysed. The following runs have been used (flagged as 1 (good runs) in RCT):

170593, 170572, 170388, 170387, 170315, 170313, 170312, 170311, 170309, 170308, 170306, 170270, 170269, 170268, 170230, 170228, 170207, 170204, 170203, 170193, 170163, 170159, 170155, 170091, 170089, 170088, 170085, 170084, 170083, 170081, 170040, 170027, 169965, 169923, 169859, 169858, 169855, 169846, 169838, 169837, 169835, 169591, 169588, 169586, 169557, 169554, 169550, 169512, 169504, 169498, 169475, 169419, 169418, 169417, 169415, 169411, 169238, 169167, 169160, 169156, 169148, 169145, 169144, 169138, 169099, 169094, 169091, 169044, 169035, 168992, 168988, 168826, 168777, 168514, 168512, 168511, 168467, 168464, 168460, 168458, 168362, 168361, 168342, 168341, 168325, 168322, 168311, 168310, 168115, 168108, 168107, 168105, 168076, 168069, 167988, 167987, 167985, 167920, 167915

The analysis was done as a part of the "Lego Trains".

2.1.2 Monte Carlo

We used the HIJING production LHC11a10a_bis and AMPT production LHC12a11a AOD081.

2.2 Analysis software

The analysis was performed using the `AliFemto` package being a part of `AliROOT` framework (v5-03-34-AN):

http://alisoft.cern.ch/viewvc/tags/v5-03-34-AN/PWGCF/FEMTOSCOPY/.

Measured correlation functions have been fitted with the custom written software. It required the input from THERMINATOR model [3], which is a particle and event generator basing on Monte Carlo methods. The model aims to study particle production in relativistic heavy ion collisions at the energies available at RHIC and LHC. THERMINATOR uses the statistical approach to describe particle production. Also, the chemical and kinetic freeze-out are assumed to occur simultaneously (*single freeze-out model*).

The fitting program makes also use of theoretical pp and pΛ correlation functions. The former one is calculated with CorrFit software [4], which compares the measured correlation function and a model one calculated using Lednicky's weights, experimental distribution of particles' momenta and an assumed emission source distribution via χ^2 test in the given range of fitting parameters. The latter one is obtained from the analytical formula of Lednicky [5], which uses the parametrization of strong interaction for pΛ system. The correlation function is calculated as the square of the wave function averaged over the total spin and over the assumed gaussian distribution of the relative distance between particle emission points in the pair rest frame.

2.3 Event selection

Events with the collision vertex position within ± 8 cm from the centre of TPC, measured along the beam axis, have been selected. The centrality selection classes are used to determine the centrality with the V0.

2.4 Particle identification

The analysis of pion femtoscopy in Pb–Pb collisions has shown that there is a need to use the so-called *TPC-only tracks* constrained to the SPD vertex (with AOD filter bit 7 set). The main reason for this is related to the fact that global tracking forces some pairs of tracks to have very similar momenta that leads to distortions in the shape of correlation functions for the lowest values of the momentum difference and, as a consequence, incorrect extracted source radii [6]. It has also been shown that the *number of* $\sigma's$ method gives more pure sample of particles than the Bayesian PID method [8]. However, *TPC-only tracks* in the AOD data files have only Bayesian PID and there is not enough information to use the $n\sigma$ method (e.g. TPC and TOF signals are missing). The solution of the above problem [7] is as follows: in AOD files, each *TPC-only track* has its equivalent amongst *global tracks* (having very similar parameters) related by:

```
tpcOnlyTrack->GetID() = - 1 - globalTrack->GetID().
```

Hence, there is a need to loop over all *global tracks* to save their indices and IDs. Afterwards, in a loop over *TPC-only tracks*, one is able to get directly a *global track* which corresponds to the current *TPC-only track* and copy the PID information. This procedure was implemented as a part of the AliFemto package. Femtoscopy analysis requires as pure sample of particles as possible but also high statistics of them. A combined TPC and TOF method was applied to select (anti)protons. The details of the cut are as follows:

- 3σ cut from TPC for tracks with TOF signal and for tracks without TOF signal for momenta less than 0.5 GeV/c
- 2σ cut from TPC for momenta in range $(0.5, 0.8)$ GeV/c for tracks without TOF signal
- maximum momentum for tracks only with TPC signal set to 0.8 GeV/c
- 3σ cut from TOF for momenta less than 1.5 GeV/c

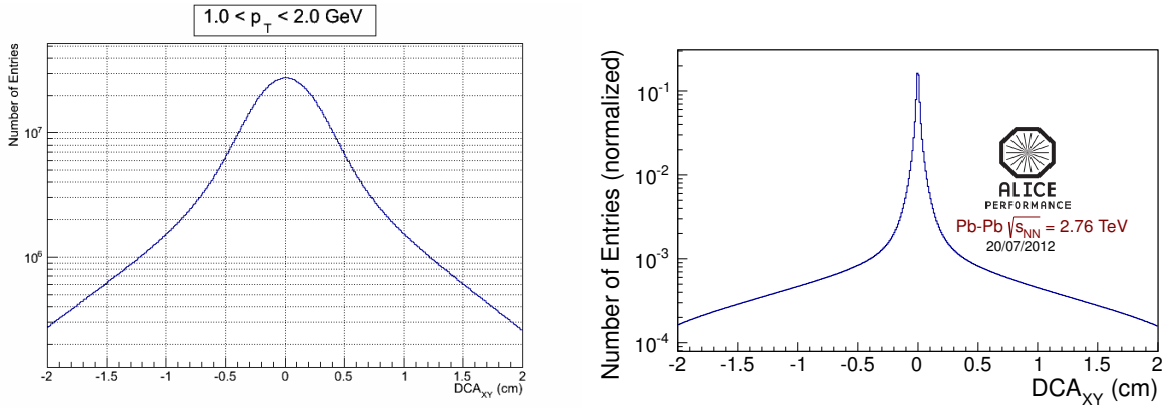

Fig. 1: The comparison of the DCA distribution in the transverse plane for *TPC-only tracks* (left panel) and *global tracks* (right panel).

– 2σ cut from TOF for momenta higher than 1.5 GeV/c

Additionally, the proton identification was adjusted with the "contour" method. It means that a given track can be identified as proton if it passes $n\sigma$ cut and its $\mathrm{d}E/\mathrm{d}x$ value for a given momentum is within the range specified by the values corresponding to the experimentally evaluated contour composed of straight lines.

2.5 Track selection

Tracks within the pseudorapidity range $\eta < |0.8|$ have been selected. To reduce contamination from material, we have chosen protons with $p_{\mathrm{t}} > 0.5$ GeV/c. For antiprotons, there are no explicit constraints on the transverse momentum. We only have limits from PID. Furthermore, the cut on a Distance of Closest Approach (DCA) was applied. Particles located within 0.1 cm in the transverse plane and 2.0 cm in the beam direction with respect to the primary vertex, were accepted. To calculate DCA values, we used `PropagateToDCA` method. It is applied for the *global tracks* corresponding to *TPC-only tracks* (similarly as with PID) because of better resolution. The comparison of the DCA distribution in the transverse plane for *TPC-only tracks* and *global tracks* is shown in Fig. 1. The cut value 0.1 cm was determined using MC simulations to obtain the highest significance. Purity of protons was estimated as 80% and of antiprotons as 84% from AMPT simulations. The DCA distribution of protons with respect to its origin from MC simulation (AMPT) is shown in Fig. 2.

The minimum number of TPC clusters corresponding to the given track was set to 80 (out of all 159 clusters). The maximum value of χ^2 per TPC cluster was 4.0 (2 degrees of freedom per cluster).

2.6 Pair selection

In case of pair selection criteria, standard cuts preventing the effects of merging (two tracks reconstructed as one) and splitting (one track reconstructed as two) were used. Strictly speaking, the cuts consists of two steps: *share quality* and *share fraction*. The former one bases on the calculation of the fraction of the number of clusters on the same TPC pad row shared by both tracks to the number of all clusters of the two tracks. Maximum *share quality* was set to 1.0 which means accepting all pairs. As regards *share fraction*, it is obtained as a ratio of shared clusters to all clusters of both tracks. All pairs sharing more than 5% clusters were rejected.

In the analysis presented in the first version of the note, a cut on angular distance [9] have not been applied. However, due to merging effects seen in correlation functions calculated from HIJING simulations (Fig. 3), the analysis with the cut was done ($\Delta\phi^* < 0.012$, $\Delta\eta < 0.015$). In Fig.4 $\Delta\phi^*\Delta\eta$ distribution from HIJING simulations is shown. Due to the necessity of the knowledge of magnetic field polarity, the

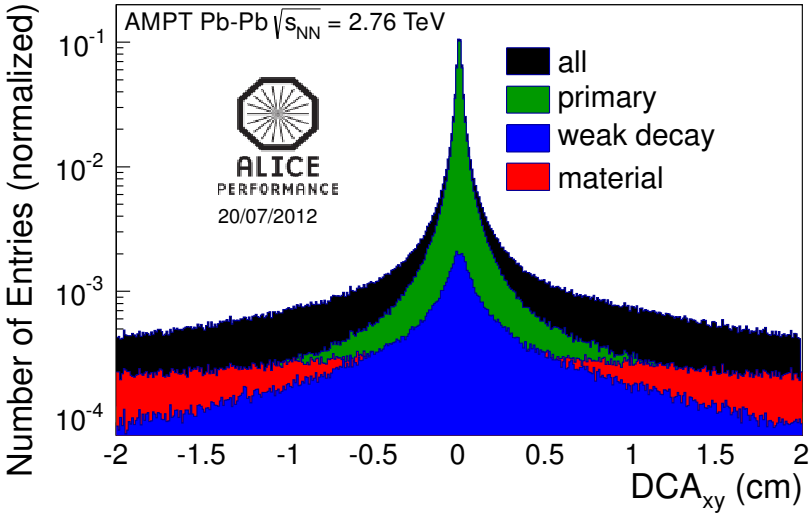

Fig. 2: The DCA distribution of protons with respect to its origin from MC simulation (AMPT).

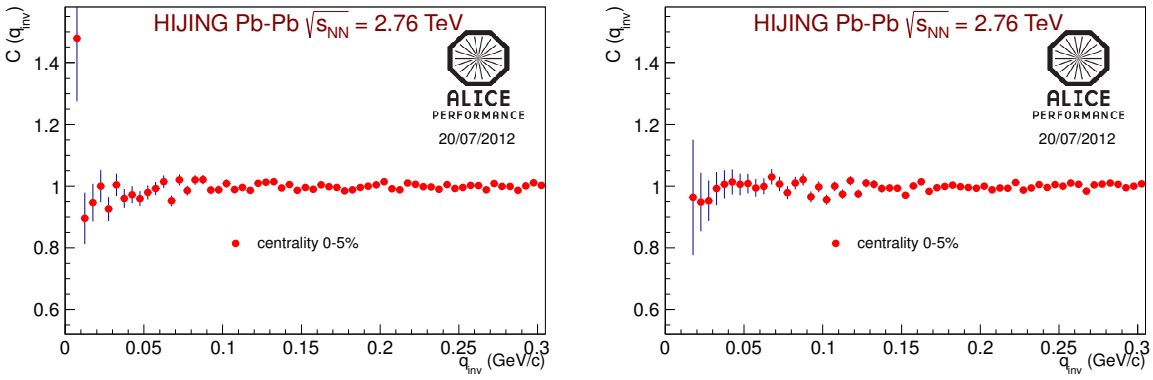

Fig. 3: pp correlation function from HIJING simulations without the cut on angular distance (left panel) and with the cut $\Delta\phi^* < 0.02$, $\Delta\eta < 0.015$.

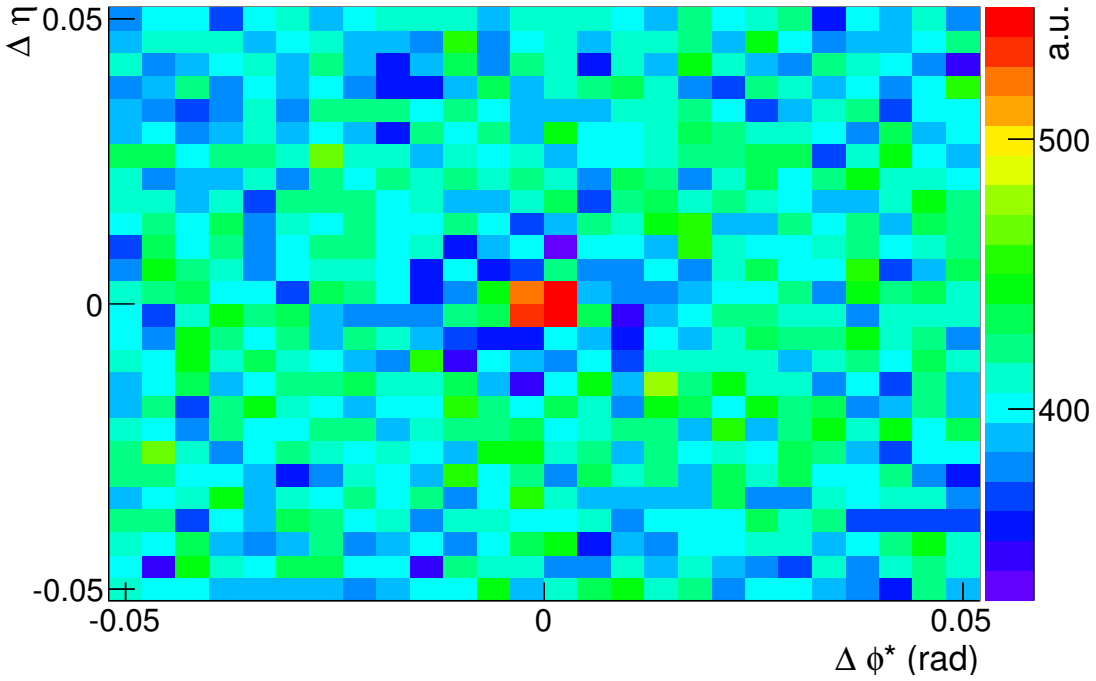

Fig. 4: $\Delta\phi^*\Delta\eta$ distribution from HIJING simulations.

analysis need to be performed for *field* $--$ and *field* $++$ runs separately. However, obtained correlation functions are consistent, so we use all runs together, to have bigger statistics.

2.7 Correlation functions

Two-particle correlations were studied in one dimensional representation with respect to the relative momentum $q_{\text{inv}} = 2 \cdot k^* = \sqrt{(p_1 - p_2)^2 - (E_1 - E_2)^2}$. The correlation effect was measured with the function defined as:

$$C(q_{\text{inv}}) = \frac{A(q_{\text{inv}})}{B(q_{\text{inv}})}, \tag{1}$$

where $A(q_{\text{inv}})$ is a distribution of correlated pairs of particles (coming from the same event), $B(q_{\text{inv}})$ is a distribution of uncorrelated pairs of particles (coming from different events - 10 events were used to create the background distribution).

The analysis has been performed for six centrality bins ($0-5\%$, $5-10\%$, $10-20\%$, $20-30\%$, $30-40\%$, $40-50\%$) and then merged into three classes: $0-10\%$, $10-30\%$ and $30-50\%$. Also, correlation functions have been calculated for two bins of the pair transverse momentum $k_{\text{t}} = (|\vec{p}_{\text{T},1} + \vec{p}_{\text{T},2}|)/2$: $0.3 < k_{\text{t}} < 1.0$ GeV/c and $k_{\text{t}} > 1.0$ GeV/c. Results for pp pairs are shown only for the second bin of k_{t} (due to not clear effects seen for the first bin, possibly caused by secondary protons). Results for $\bar{\text{p}}\bar{\text{p}}$ are shown for the merged two k_{t} bins and for the second bin, whereas for $\text{p}\bar{\text{p}}$: only for the merged two k_{t} bins.

3 Results

In Fig. 5, 6, 7 and 8 the correlation functions of pp, $\bar{\text{p}}\bar{\text{p}}$ and $\text{p}\bar{\text{p}}$ systems are presented. In case of identical systems, the expected maximum due to strong interactions for $q_{\text{inv}} \approx 40$ MeV/c is clearly visible. The results reveal that proton-proton and antiproton-antiproton correlations are consistent. Also, the centrality dependence is understandable - the more peripheral the events, the stronger the correlation effect is.

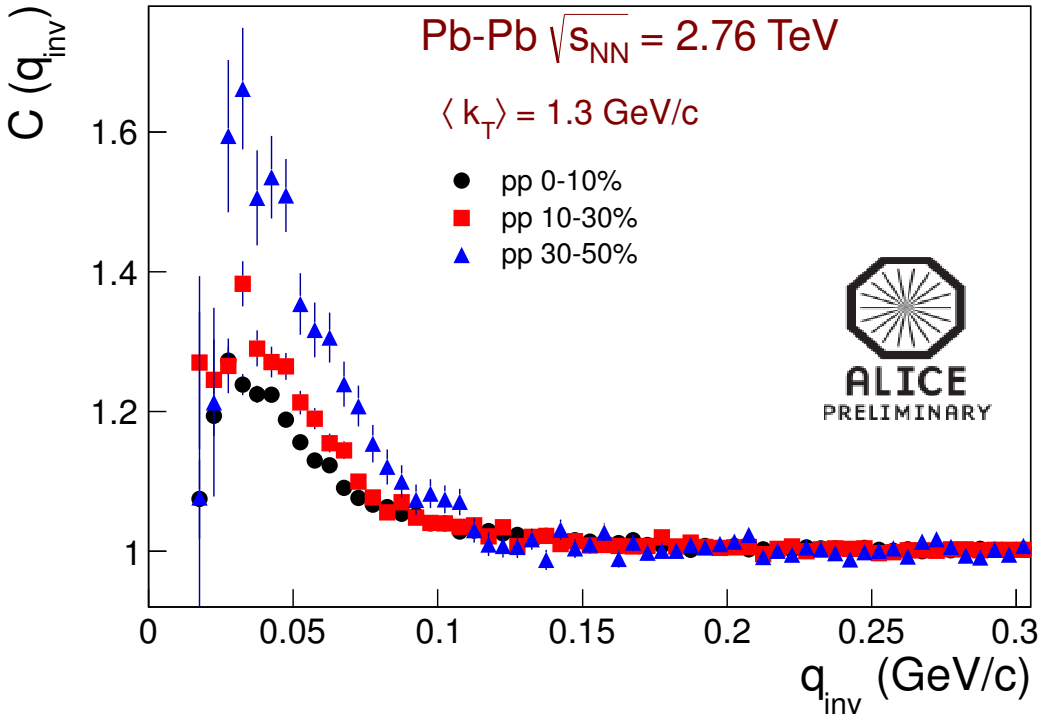

Fig. 5: Proton-proton correlation functions for the $\sqrt{s_{NN}} = 2.76$ TeV Pb–Pb collision data.

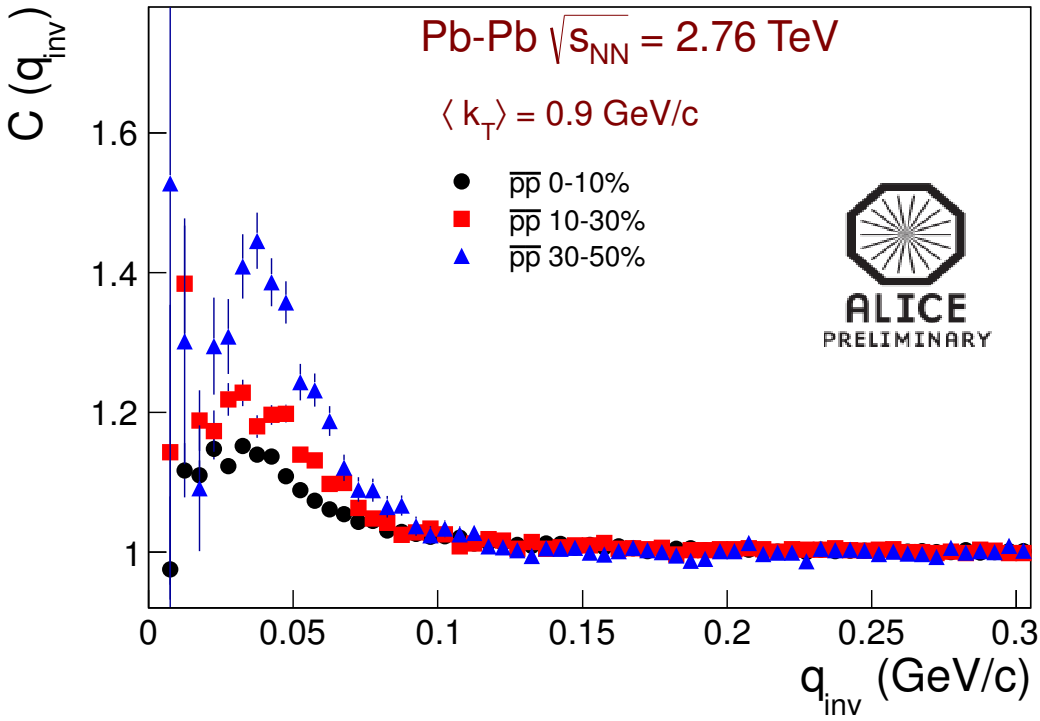

Fig. 6: Antiproton-antiproton correlation functions for the $\sqrt{s_{NN}} = 2.76$ TeV Pb–Pb collision data ($\langle k_t \rangle = 0.9$ GeV/c).

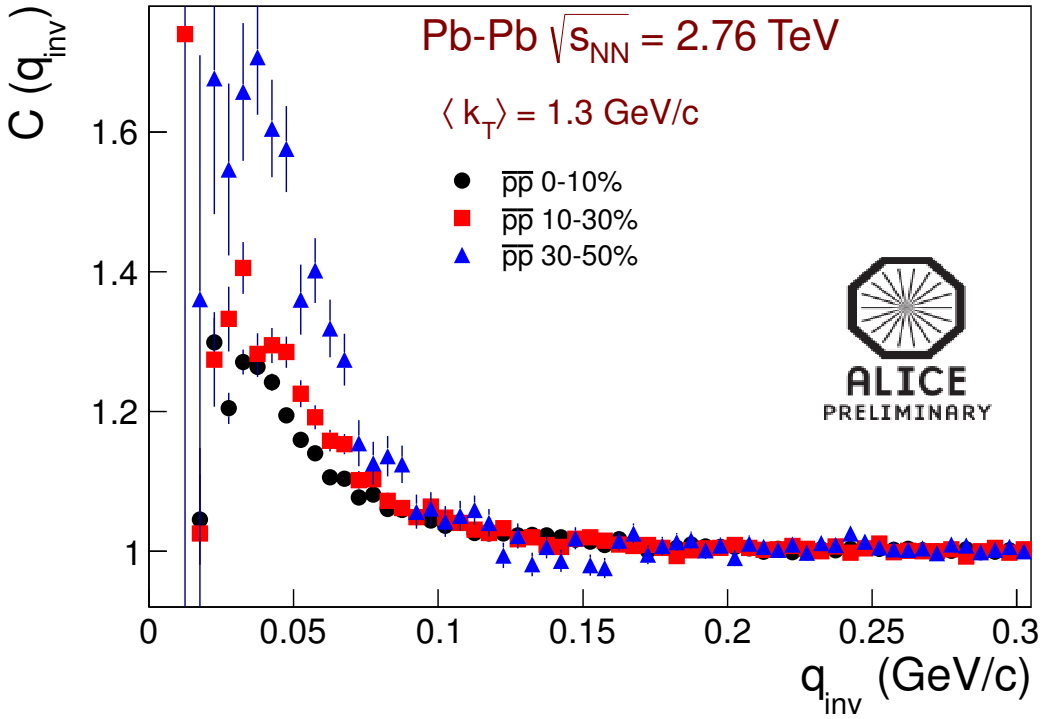

Fig. 7: Antiproton-antiproton correlation functions for the $\sqrt{s_{NN}} = 2.76$ TeV Pb–Pb collision data ($\langle k_t \rangle = 1.3$ GeV/c).

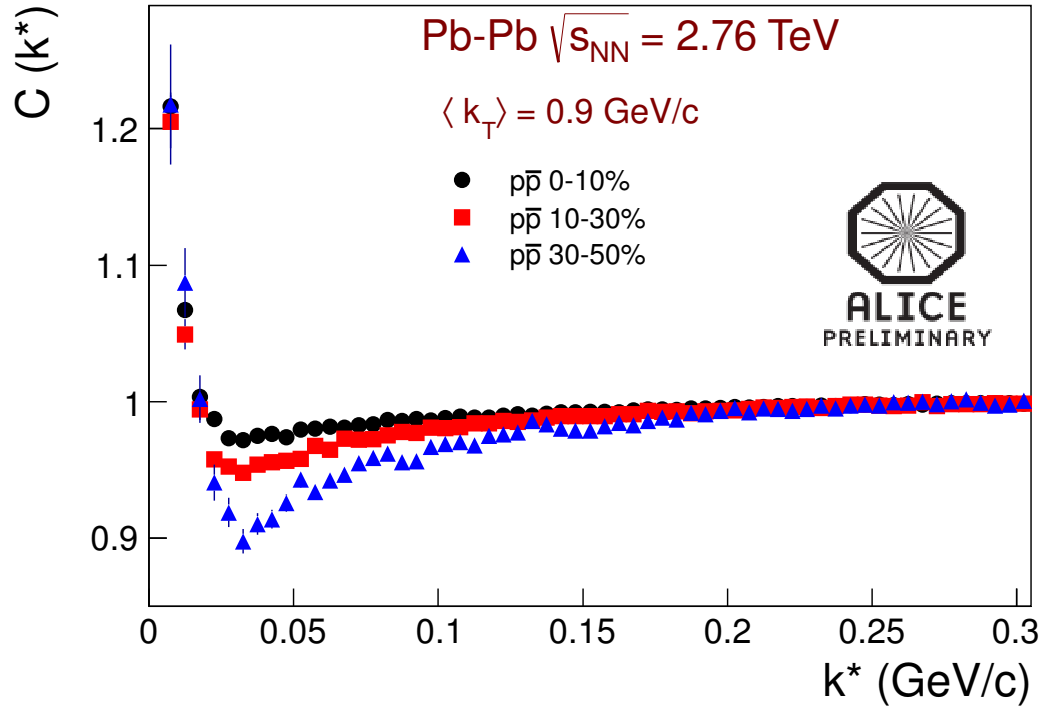

Fig. 8: Proton-antiproton correlation functions for the $\sqrt{s_{NN}} = 2.76$ TeV Pb–Pb collision data.

It means that the size of the emitting source is growing with multiplicity. Proton-antiproton correlations show expected behaviour - a maximum for the lowest momentum difference due to Coulomb attraction, then a minimum caused by the annihilation processes. Another observed feature is the flat background of the correlation function at large values of momentum difference which indicates the absence of wide non-femtoscopic structures.

In Fig. 9 the correlation functions are compared with those calculated without the cut on angular distance. Differences are within statistical errors.

In Fig. 10 the comparison of correlation functions calculated for "field $--$" and "field $++$" runs is shown. The only visible difference can be noticed for proton-antiproton correlation function (centrality $0-10\%$). However, radii fitted for these functions are within statistical and systematic errors shown below.

Fitting the correlation functions for proton systems can be performed with the software package `CorrFit`. However, as it can be seen in Fig. 11, attempts to fit the obtained correlation functions directly with `CorrFit` failed. Correlation of pp pairs has three components. The Coulomb and quantum statistics have to be negative (e.g. give the correlation function below unity). The strong interaction is positive but has limited width - one can think of it as a resonance peak. Therefore, the excess in the range $30-80$ MeV/c of k^* cannot be explained by correlations coming from the pp wave function. A significant influence of residual correlations may be a possible explanation. As the influence of residual correlations seems to be significant, the method of simultaneous fitting of pp ($\bar{\mathrm{p}}\bar{\mathrm{p}}$) and p$\Lambda$ ($\bar{\mathrm{p}}\bar{\Lambda}$) correlations was proposed. It is assumed that residual correlations coming from pΣ^+ system are negligible, due to a known small cross-section for this system. Hence, the experimental correlation function of pp and $\bar{\mathrm{p}}\bar{\mathrm{p}}$ systems were fitted with the formula:

$$C_{meas}(k^*_{pp}) = 1 + \lambda_{pp} \cdot (C_{pp}(k^*_{pp};R) - 1) + \lambda_{p\Lambda} \cdot (C_{p\Lambda}(k^*_{pp};R) - 1), \tag{2}$$

where:

- λ_{pp}, $\lambda_{p\Lambda}$ - parameters which describes the relative number of pp pairs where both particles are primary (λ_{pp}) and pairs where one particle is primary, the other is a product of Λ decay ($\lambda_{p\Lambda}$),
- R - radius
- $C_{pp}(k^*_{pp};R)$ - theoretical proton-proton correlation function for given R (Gaussian source assumed), obtained from `CorrFit`,
- $C_{p\Lambda}(k^*_{pp};R) = \sum_{k^*_{p\Lambda}} C_{p\Lambda}(k^*_{p\Lambda}) T(k^*_{pp},k^*_{p\Lambda})$ - theoretical pΛ correlation function for given R obtained from Lednicky's model,
- $T(k^*_{pp},k^*_{p\Lambda})$ - transformation factors related to Λ decay kinematics, calculated with `THERMINATOR`.

The pΛ correlation function obtained with Lednicky's model is calculated as a function of $k^*_{p\Lambda}$, but according to Eq. (2), there is a need to use $C_{p\Lambda}$ dependent on the relative momentum between two protons. Therefore, relevant transformation should be performed, namely for each value of k^*_{pp}, $C_{p\Lambda}$ is determined as a sum over all $k^*_{p\Lambda}$ values of $C_{p\Lambda}$ obtained with Lednicky's model scaled by factors from the two-dimensional histogram $T(k^*_{pp},k^*_{p\Lambda})$ calculated with `THERMINATOR`:

$$C_{p\Lambda}(k^*_{pp};R) = \sum_{k^*_{p\Lambda}} C_{p\Lambda}(k^*_{p\Lambda}) T(k^*_{pp},k^*_{p\Lambda}). \tag{3}$$

The kinematics dependence of Λ decay $T(k^*_{pp},k^*_{p\Lambda})$ is shown in Fig. 12. Fig. 13 shows an example of the transformation of $C_{p\Lambda}$.

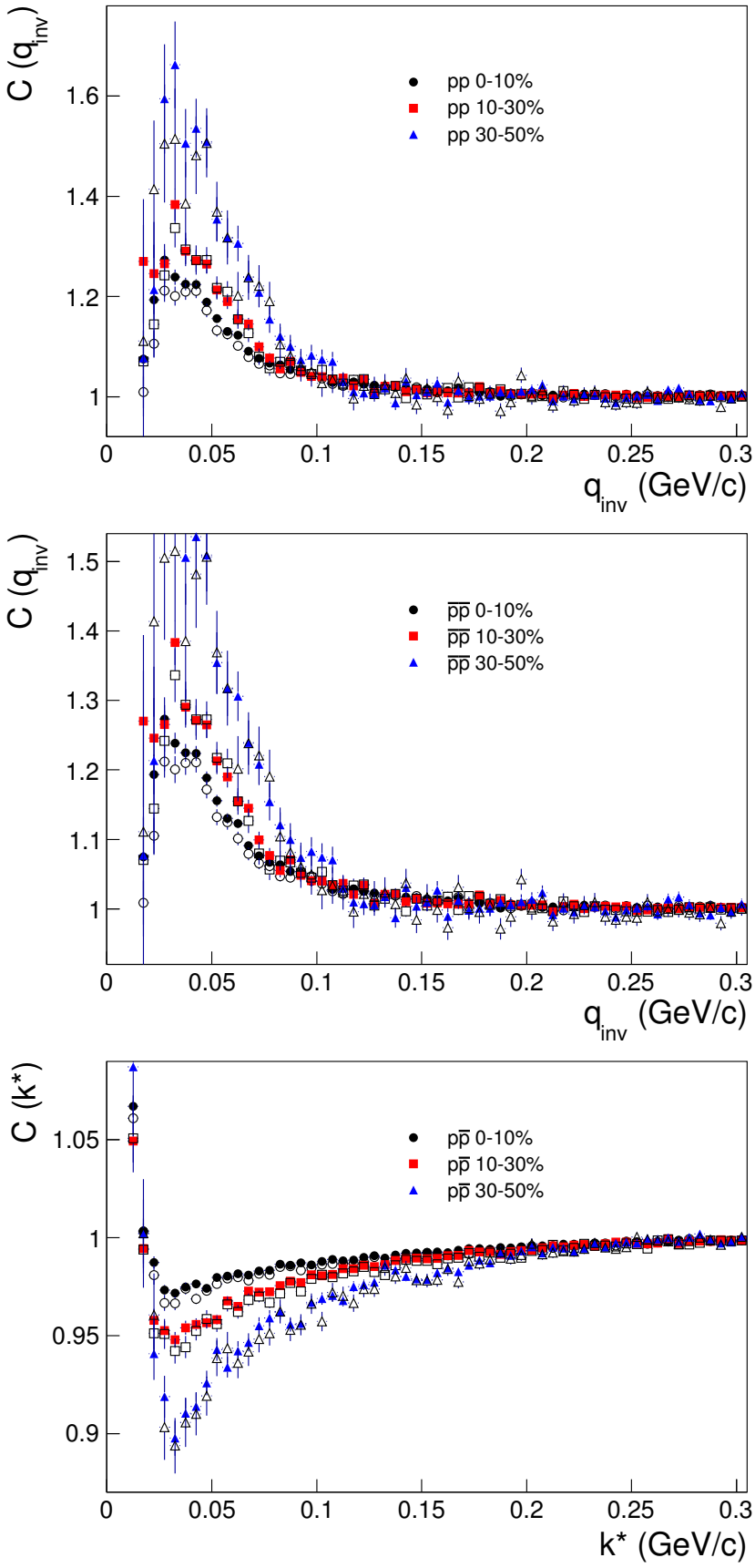

Fig. 9: From top to bottom: proton-proton, antiproton-antiproton and proton-antiproton correlation functions. Results before (open markers) and after (solid markers) applying the cut on angular distance are shown.

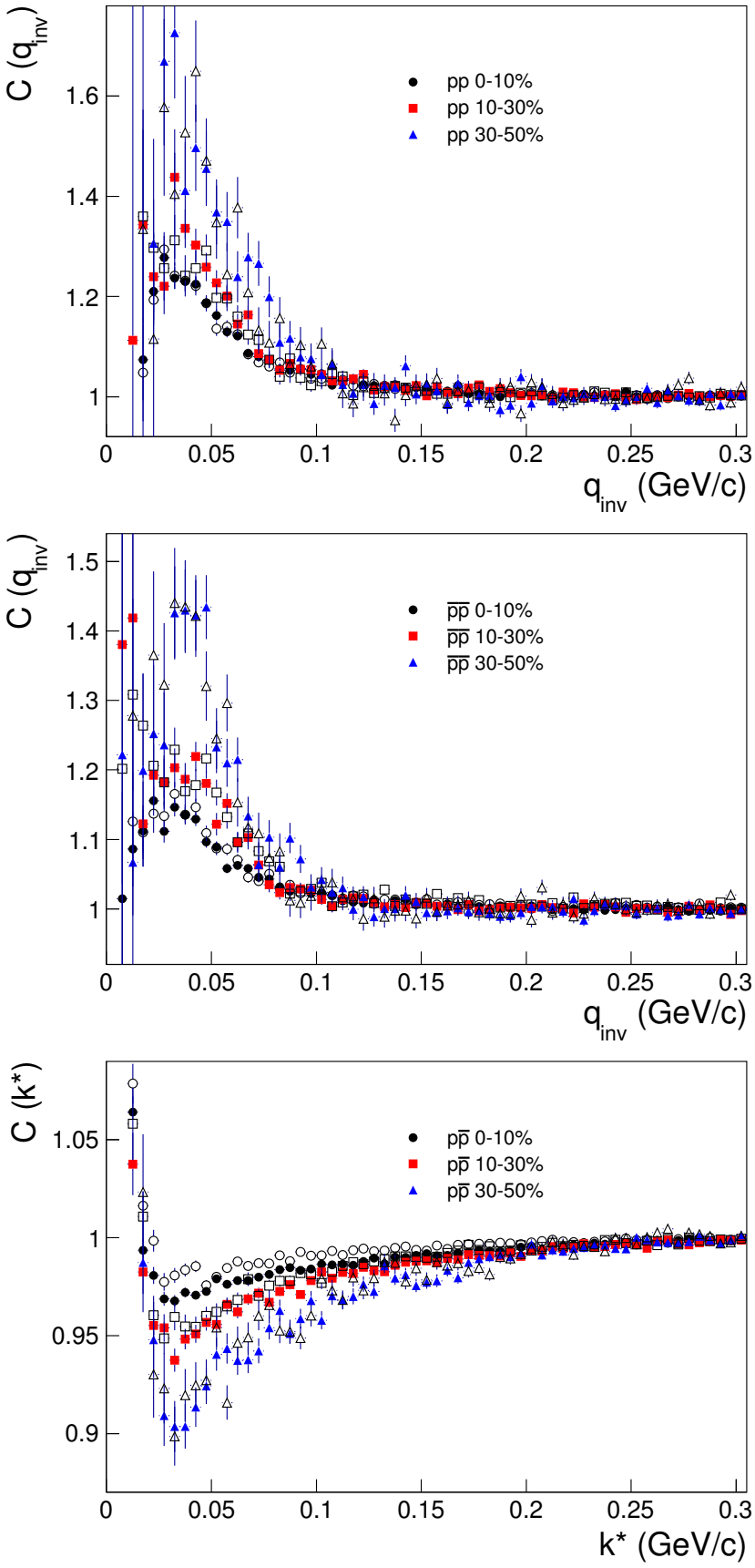

Fig. 10: From top to bottom: proton-proton, antiproton-antiproton and proton-antiproton correlation functions. Results for "field ++" runs (open markers) and "field −−" runs (solid markers) are shown.

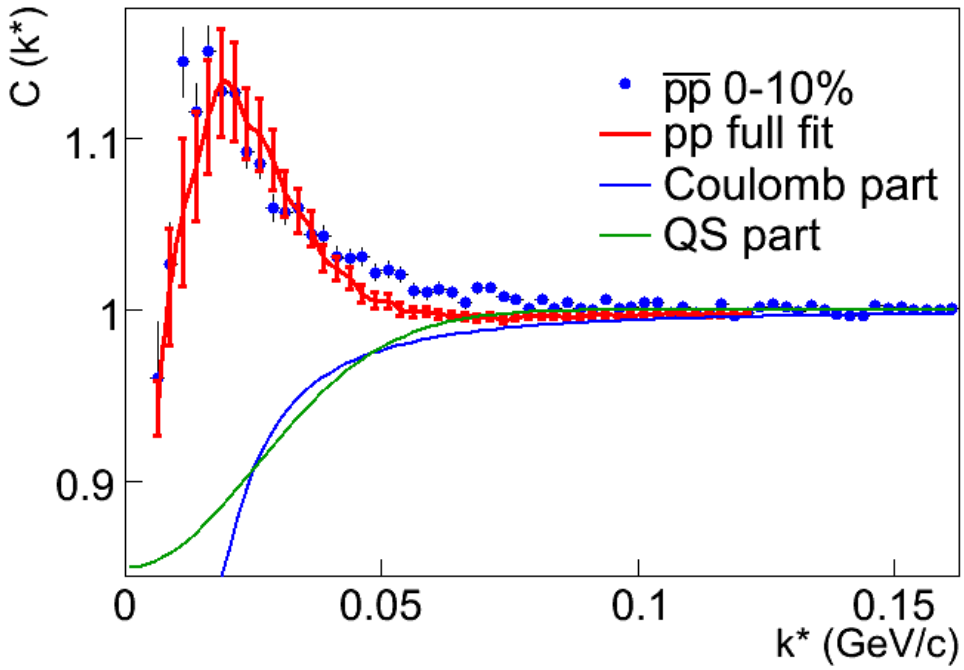

Fig. 11: Comparison of experimental correlation functions and fit obtained with `CorrFit` [4]. Contribution of Coulomb repulsion and Quantum Statistics are also shown [5].

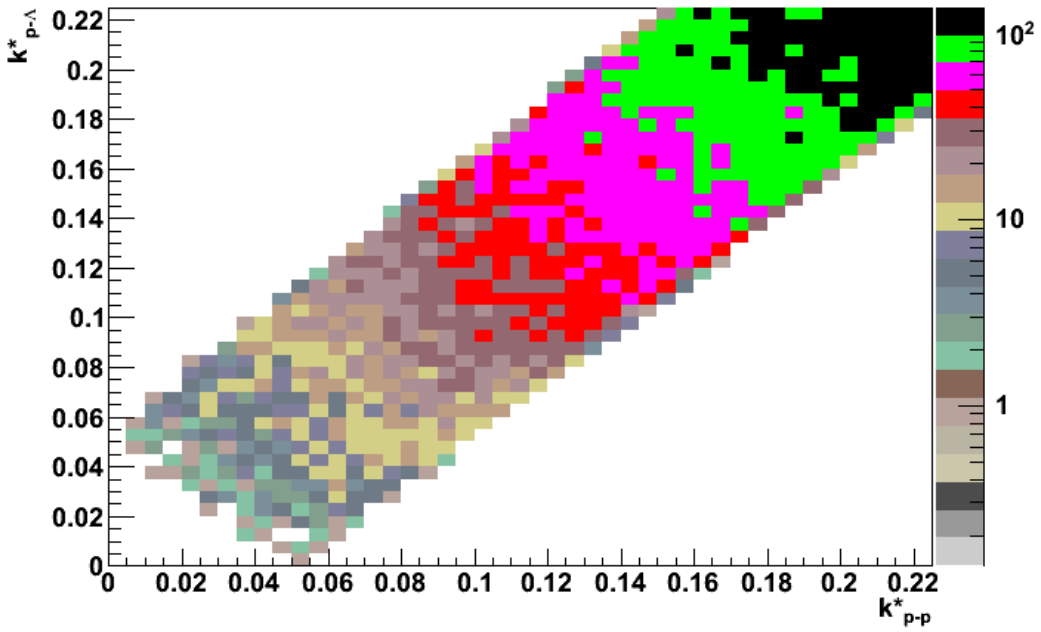

Fig. 12: Kinematics dependence of Λ decay $T(k^*_{pp}, k^*_{p\Lambda})$ calculated with `THERMINATOR`.

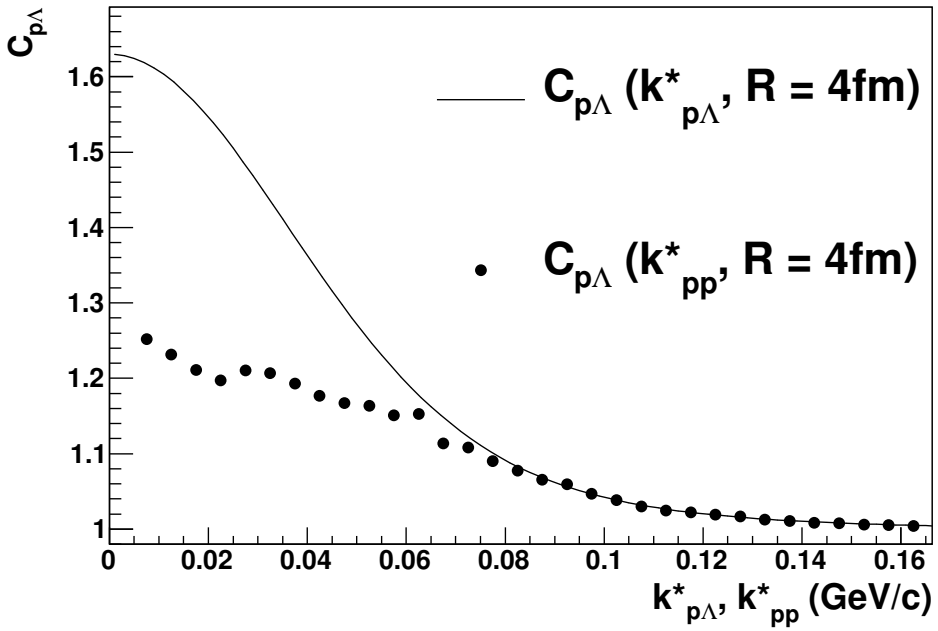

Fig. 13: Example of the transformation of $C_{p\Lambda}(k^*_{p\Lambda}) \rightarrow C_{p\Lambda}(k^*_{pp})$.

As far as fitting the p$\bar{\text{p}}$ correlations are concerned, the relevant formula is analogous to Eq. (2) and takes the following form:

$$C_{meas}(k^*_{p\bar{p}}) = 1 + \lambda_{p\bar{p}} \cdot (C_{p\bar{p}}(k^*_{p\bar{p}}; R) - 1) + \lambda_{\bar{p}\Lambda} \cdot (C_{\bar{p}\Lambda}(k^*_{p\bar{p}}; R) - 1). \quad (4)$$

The $\bar{\text{p}}\Lambda$ correlation function calculated with the analytical model of Lednicky and Lyuboshitz and its form after the transformation to the reference frame of two protons (one of which comes from Λ decay) are shown in Fig. 14.

pp (p$\bar{\text{p}}$) and pΛ ($\bar{\text{p}}\Lambda$) correlation functions have been calculated for the emission radii from 1.0 fm to 6.0 fm with a step of 0.1 fm. A gradient minimisation algorithm is used to find a minimum χ^2 value calculated between the experimental correlation function and the functions defined by Eq. (2) and (4) calculated for given parameters λ_{pp}, $\lambda_{p\Lambda}$ ($\lambda_{p\bar{p}}$, $\lambda_{\bar{p}\Lambda}$) and R by the quadratic interpolation of the theoretical correlation functions. It is assumed that the radii of pp (p$\bar{\text{p}}$) and pΛ ($\bar{\text{p}}\Lambda$) sources are equal.

Fig. 15 and 16 are the examples of the fitting results for $\bar{\text{p}}\bar{\text{p}}$ and p$\bar{\text{p}}$ correlation functions. The fit qualitatively works, namely contribution from pp correlations describes the maximum at $k^* \approx 20$ MeV/c and wide background of the functions is reproduced by residual correlations coming from pΛ system.

We found following sources of the systematic errors:

- constraints on the λ_{pp}, $\lambda_{p\Lambda}$ parameters
  - fixing the ratio $\lambda_{pp}/\lambda_{p\Lambda}$ to values estimated from other fits caues the maximum change of the radius 13% (usually $< 5\%$)
  - fixing to estimates from AMPT (see Tab.1): in general, fit fails
- fitting procedure
  - ranges of the fit and starting parameters - changing the fit range by $\pm 10\%$ causes the maximum change less than 6% for the radius (usually $< 2\%$)

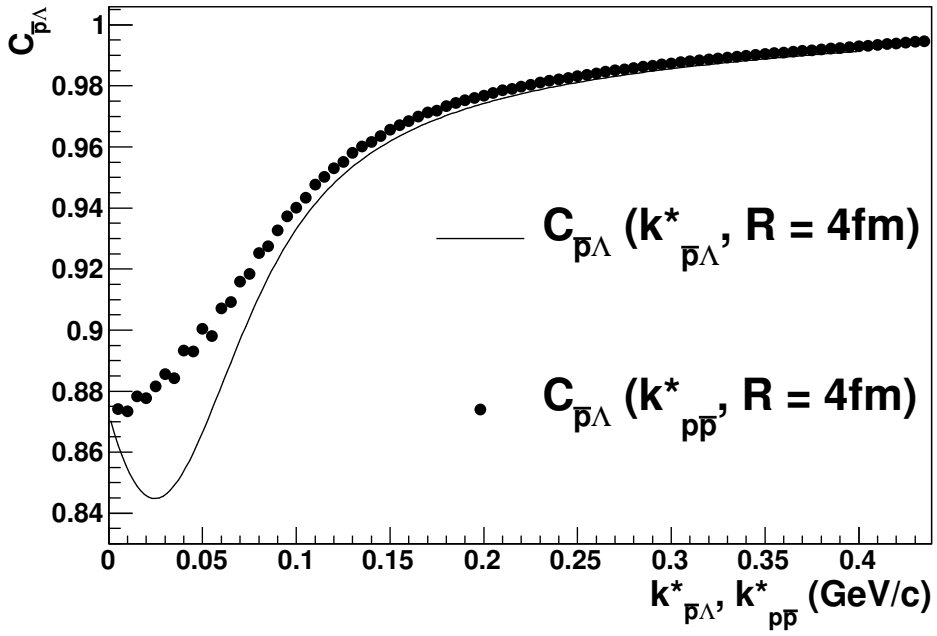

Fig. 14: The $\bar{p}\Lambda$ correlation function calculated with the analytical model of Lednicky and Lyuboshitz and its form after the transformation: $C_{\bar{p}\Lambda}(k^*_{\bar{p}\Lambda}) \rightarrow C_{\bar{p}\Lambda}(k^*_{p\bar{p}})$.

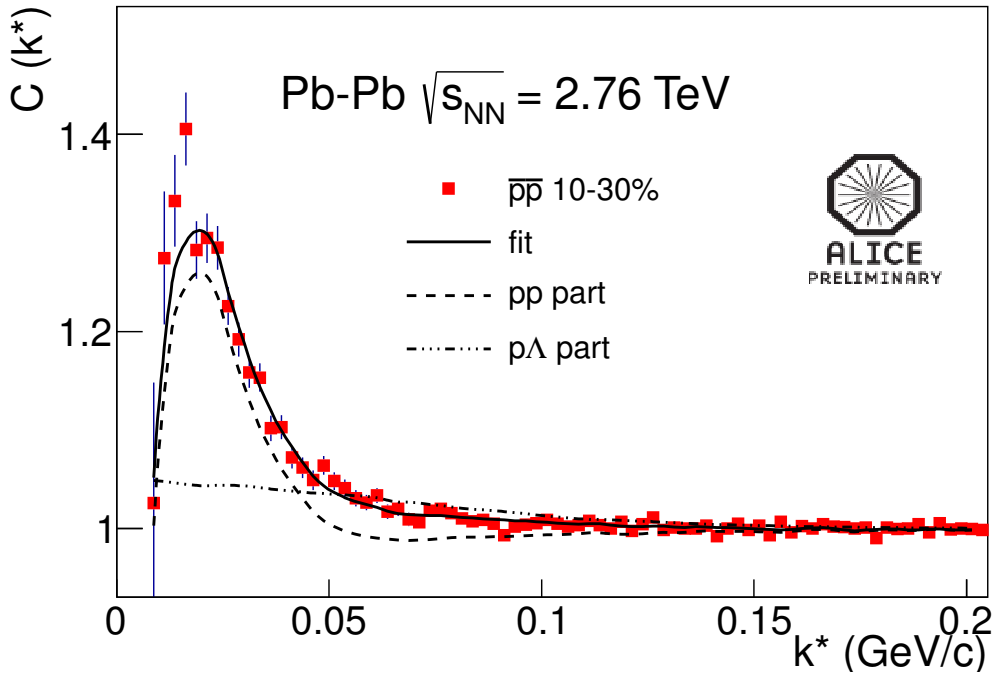

Fig. 15: Results of the fitting the $\bar{p}\bar{p}$ correlation function. The contribution of the theoretical pp and pΛ correlation functions scaled by factors related to the relevant fractions of pp pairs are shown with dashed and dotted-dashed lines, respectively.

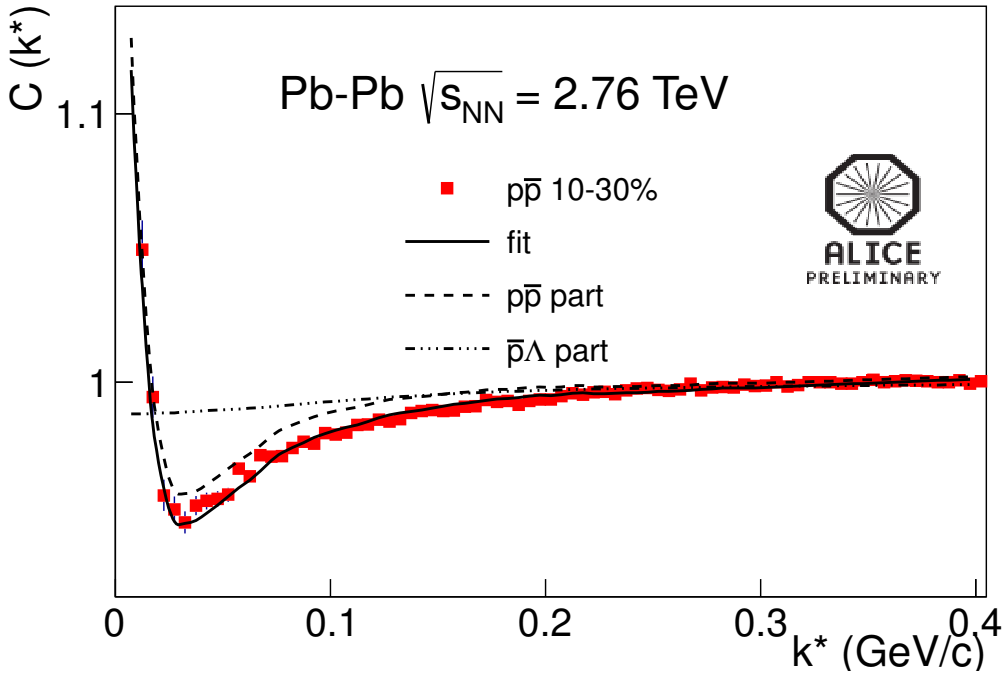

Fig. 16: Results of the fitting the pp̄ correlation function. The contributions of the theoretical pp̄ and p̄Λ correlation functions scaled by factors related to the relevant fractions of pp̄ pairs are shown with dashed and dotted-dashed lines, respectively.

- stability of the numerical fit - $< 10\%$ (usually $< 3\%$)
- assumption regarding $R_{p\Lambda}/R_{pp}$ ratio (following m_t scaling from hydrodynamics) - taking $R_{p\Lambda} = 0.95R_{pp}$ causes the change of the radius less than 1%
- influence of the two track cuts (ϕ^*) - $< 10\%$ (usually $< 4\%$)

Systematic error for given system, centrality and k_t bin is estimated as the maximum error within each system. Maximum systematic error for the radius is estimated as: $+20\%$, -21%.

	HIJING		AMPT	
	p	p̄	p	p̄
primary	53%	85%	57%	75%
Λ ($\bar{\Lambda}$) decay	6%	11%	9%	17%
Σ^+ ($\bar{\Sigma}^+$) decay	2%	2%	3%	7%
rest	39%	2%	31%	1%

Table 1: Fractions of (anti)protons with respect to its origin from MC simulations.

Tab. 2 contains the numerical values of the fitted radii with statistical and systematic errors. Fig. 17 shows the monotonic centrality dependence of the fitted radii for all combinations of pairs of (anti)protons. Fig. 18 shows the radii from proton femtoscopy as a function of charged particle density.

In Fig. 19 radii obtained in proton femtoscopy as well as those extracted from $\pi\pi$, $K^{\pm}K^{\pm}$ and $K^0_S K^0_S$ correlations are plotted versus $m_t = \sqrt{\langle k_t \rangle^2 + m_0^2}$. R_{inv} is scaled by the approximate kinematic factor $(\frac{\sqrt{\gamma}+2}{3})^{-1/2}$. Hydrodynamics predicts m_t of the radii calculated in LCMS (Longitudinally Co-Moving System). However, R_{inv} is calculated in PRF (Pair Rest Frame). Therefore, approximate m_t scaling may

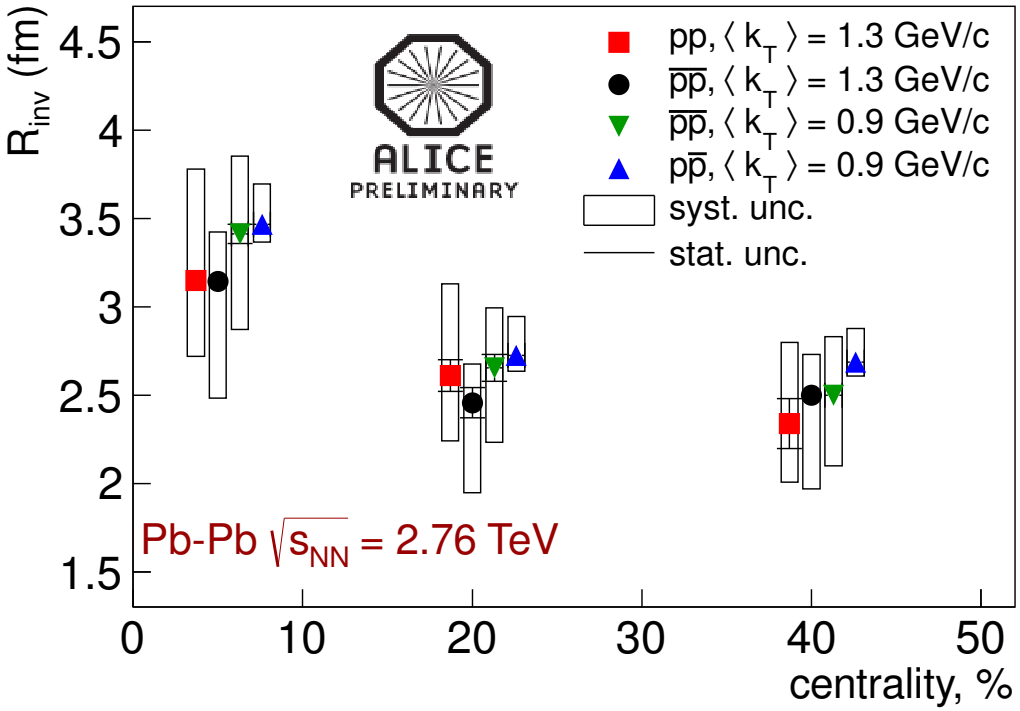

Fig. 17: Centrality dependence of the fitted radii from proton femtoscopy. Statistical (lines) and systematic (boxes) errors are shown.

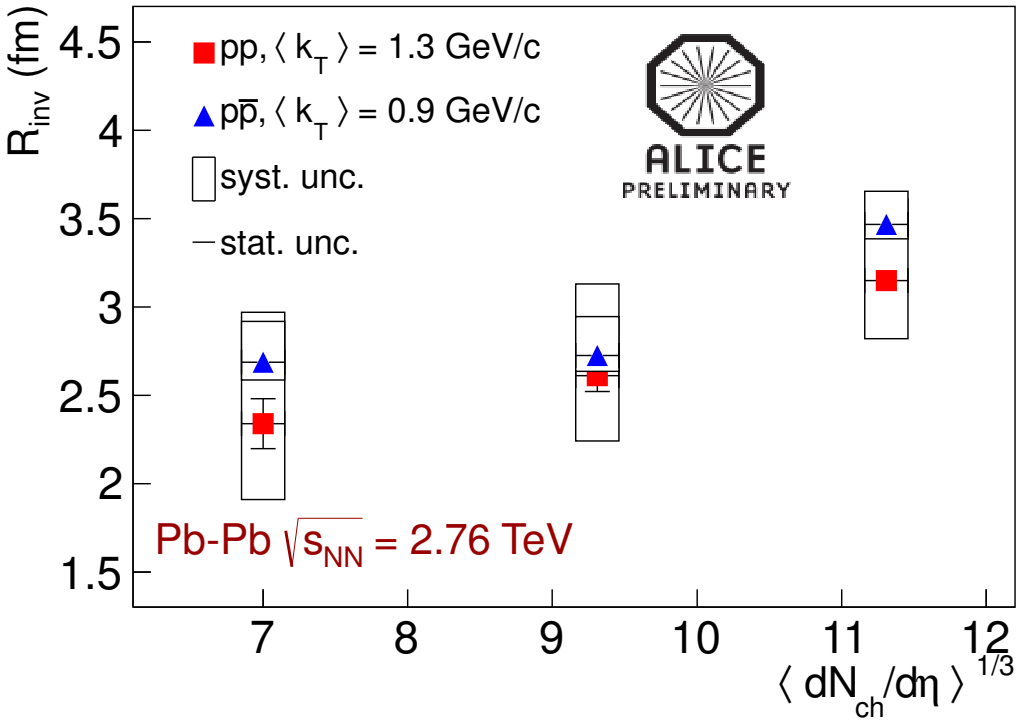

Fig. 18: Radii from proton femtoscopy vs. charged particle density. Statistical (lines) and systematic (boxes) errors are shown.

	R (fm)			
	pp	$\bar{\mathrm{p}}\,\bar{\mathrm{p}}$		$\mathrm{p}\bar{\mathrm{p}}$
$\langle k_{\mathrm{t}} \rangle$ (GeV/c)	1.3	0.9	1.3	0.9
0-10%	$3.15 \pm 0.05^{+0.63}_{-0.43}$	$3.41 \pm 0.05^{+0.44}_{-0.54}$	$3.14 \pm 0.04^{+0.28}_{-0.66}$	$3.47 \pm 0.05^{+0.23}_{-0.10}$
10-30%	$2.61 \pm 0.09^{+0.52}_{-0.37}$	$2.65 \pm 0.08^{+0.34}_{-0.42}$	$2.45 \pm 0.09^{+0.22}_{-0.51}$	$2.73 \pm 0.02^{+0.19}_{-0.08}$
30-50%	$2.34 \pm 0.14^{+0.46}_{-0.33}$	$2.50 \pm 0.01^{+0.33}_{-0.40}$	$2.50 \pm 0.01^{+0.23}_{-0.53}$	$2.69 \pm 0.02^{+0.19}_{-0.08}$

Table 2: Radii extracted from proton femtoscopy. Statistical and systematic errors are shown, respectively.

be recovered by using the given formula. In Fig. 20 results for charged and neutral kaons as well as for (anti)protons are combined using weighted mean method:

$$R_{mean} = \frac{\sum_i R_i w_i}{\sum_i w_i}$$

$$SystErr_{mean} = \frac{\sum_i SystErr_i w_i}{\sum_i w_i} + diff$$

$$w_i = \frac{1}{\sigma_i^2}$$

where σ_i - statistical error, $diff$ - the difference in radius between different pair types. Results for kaons are combined in the following way:

- 1.-4. m_{t} bins $K^{ch}K^{ch}$ + 1. m_{t} bin $K^0_S K^0_S$
- 5.-6. m_{t} bins $K^{ch}K^{ch}$ + 2. m_{t} bin $K^0_S K^0_S$
- 7. m_{t} bin $K^{ch}K^{ch}$ + 3. m_{t} bin $K^0_S K^0_S$
- 4. m_{t} bin $K^0_S K^0_S$

For protons, we combined the first m_{t} bins for $\mathrm{p}\bar{\mathrm{p}}$ and $\bar{\mathrm{p}}\bar{\mathrm{p}}$ and the second m_{t} bins for pp and $\bar{\mathrm{p}}\bar{\mathrm{p}}$.

4 Summary

In summary, correlations of all combinations of pairs of protons and antiprotons have been measured in Pb–Pb collisions at $\sqrt{s_{NN}} = 2.76$ TeV in the ALICE experiment. The femtoscopic parameters for the radius of the proton source are extracted from one-dimensional pp, $\bar{\mathrm{p}}\bar{\mathrm{p}}$ and $\mathrm{p}\bar{\mathrm{p}}$ correlation functions. The fit includes final-state interactions and quantum statistics for identical pairs of (anti)protons. What is more, the fit takes into account residual correlations coming from pΛ system. Two-proton correlations show an increase of the radius with increasing multiplicity and slight decrease of the radius with increasing pair transverse momentum.

References

[1] The ALICE Collaboration: *Two-pion Bose-Einstein correlations in central PbPb collisions at* $\sqrt{s_{NN}} = 2.76$ *TeV*; Phys.Lett.B696:328-337,2011

[2] Gos, H. P. for the STAR collaboration : *Proton - proton, anti-proton - anti-proton, proton - anti-proton correlations in Au+Au collisions measured by STAR at RHIC*; Eur.Phys.J. C49 (2007) 75-80

[3] Kisiel, A., Taluc, T., Broniowski W., Florkowski, W.; *THERMINATOR: THERMal heavy-IoN generATOR*; Comput.Phys.Commun. 174 (2006) 669-687

[4] Kisiel, A.: *CorrFit - a program to fit arbitrary correlation functions*; Nukleonika 49;Suppl 2:s81-s83 (2004)

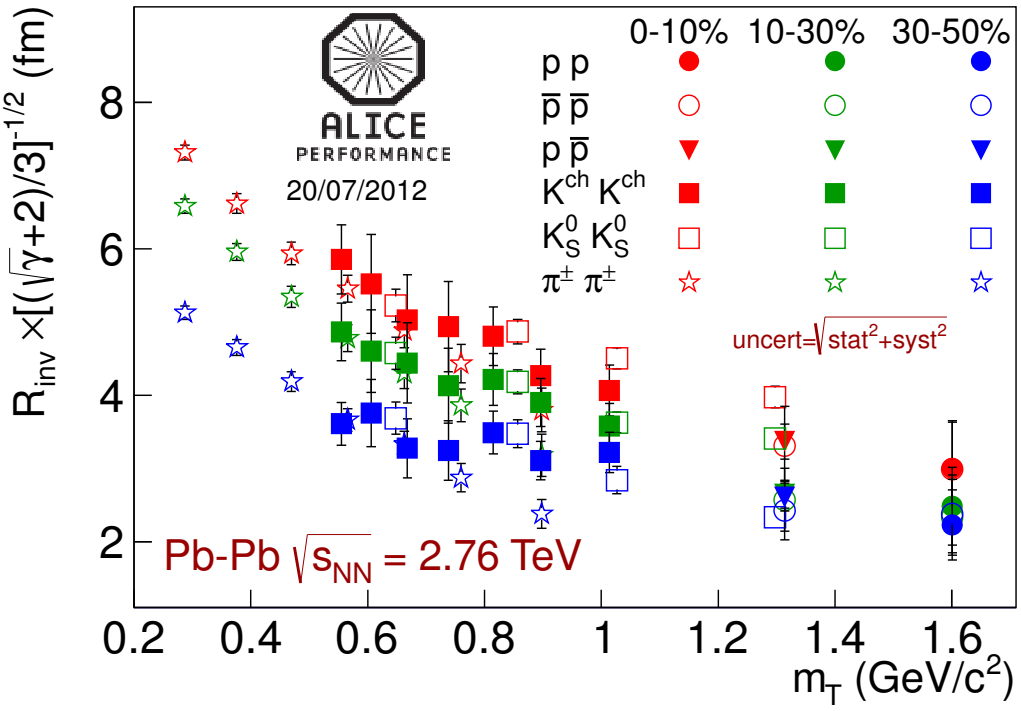

Fig. 19: m_t dependence of the radius parameter extracted from correlations of pions, charged kaons, neutral kaons and protons. Estimates of total errors (the quadrature sum of the statistical and the systematic ones) are shown.

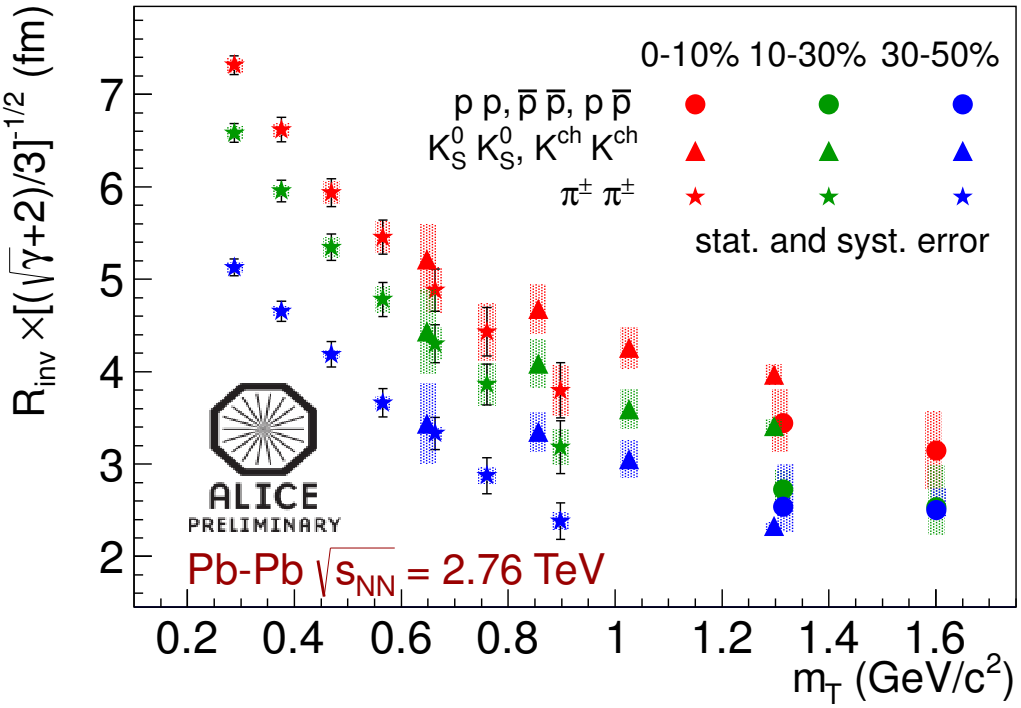

Fig. 20: m_t dependence of the radius parameter extracted from correlations of pions, charged kaons, neutral kaons and protons. Results for charged and neutral kaons as well as for (anti)protons are combined using weighted mean method (see text for details).

[5] Lednicky, R.: *Finite-size effects on two-particle production in continuous and discrete spectrum*; Phys.Part.Nucl. 40 (2009) 307-352

[6] The LHC Computing Grid software development portal Savannah: `https://savannah.cern.ch/bugs/?func=detailitem&item_id=75267`

[7] Christian Klein-Boesing, private communication

[8] Malinina, L.: `https://indico.cern.ch/getFile.py/access?contribId=22&sessionId=6&resId=0&materialId=slides&confId=147108`

[9] Gramling, J.L. `http://indico.cern.ch/getFile.py/access?contribId=42&sessionId=16&resId=0&materialId=slides&confId=146554`